Elemental abundances of the low corona as derived from SOHO/CDS observations

G. Del Zanna*, B.J.I. Bromage† and H.E. Mason*

*DAMTP, University of Cambridge, Cambridge, UK
†Centre for Astrophysics, University of Central Lancashire, UK

Abstract. Some of the main factors that affect the determination of the element abundances from EUV spectra are reviewed. The ionization balance, the selection of lines, and the spectroscopic method used can each account for a variation of a factor of two or more in the derived element abundances, in particular cases. Diagnostic techniques are applied to Skylab/HCO and SOHO/CDS observations of solar coronal holes and plumes, in order to derive their relative element abundances. It is confirmed that coronal holes have photospheric abundances, while plumes only show a small FIP effect, contrary to what has long been thought. It is shown that the plume characteristics can mainly be explained in terms of their temperature structure rather than a large FIP effect.

INTRODUCTION

A correlation between the coronal abundances of some solar regions and the first ionization potential (FIP) of the various elements (e.g., see the review of Raymond et al. [1]) has been found by many authors. A large variety of coronal abundances have been reported, with differences from the photospheric values that usually range from 2 to 4, except for extreme cases.

In the past, using Skylab S-082A observations, only a limited number of lines could be used unambiguously, due to the characteristics of the overlapping spectroheliograms. Most results were based on observations of Mg VI and Ne VI lines, selected as representatives of a low- and a high-FIP element, respectively. Although the observed intensity ratios of lines from these ions do show large variations for different coronal structures, it is not straightforward to deduce variations in relative element abundances. In fact, various other effects can change the observed ratios, as discussed below.

Recently, the spectroscopic instruments on board SOHO, have provided a new opportunity to study in detail the chemical composition of the solar transition region and corona. Here, we are primarily concerned with spectroscopic measurements of relative abundances, and with the various factors that can affect the determination of the element abundances. These factors can be broadly grouped into the following classes:

1. The diagnostic method used.
2. The selection of spectral lines used.
3. The assumption of ionization equilibrium and the ionization balance used.
4. The atomic data used for each ion.
5. Temperature and density effects.
6. Instrument calibration.

Previously, other authors [2, 3, 4] have pointed out that some of these factors may have led to inaccurate determinations of the element abundances. The problems summarised here are general, that is are not instrument dependent, since they have been found in Skylab, SOHO, and other data. More details can be found in [5]. Here, only a few examples are given, to point out that some of these factors can account for large variations (of a factor of 2-3) in the derived element abundances.

In this paper we present results from the Coronal Diagnostic Spectrometer (CDS) on SOHO [6] which consists of two spectrometers (a Normal Incidence, NIS; and a Grazing Incidence, GIS) and six channels, covering almost entirely the 151-785 Å wavelength region. The CDS observations have many advantages in reducing some of the uncertainties listed above. One of the key issues is the CDS ability to observe many emission lines from a large number of highly ionized ions of the most abundant elements. These cover a large range of temperatures and isoelectronic sequences. The CDS radiometric calibration was uncertain during the first period of the mission. This produced large uncertainties (factor of 2-3) in some earlier element abundance measurements (e.g., Mg/Ne, see [7]). However, the CDS instrument is now well calibrated [8] within 20-30%, which is of the same order as the accuracy of the atomic data.

THE DIAGNOSTIC METHODS

The intensity $I(\lambda_{ij})$, of a spectral line emitted by an optically thin plasma can be written as in [1]:

$$I(\lambda_{ij}) = A_b(X) \int C(T,\lambda_{ij},N_e)\, N_e\, N_H\, dh \qquad (1)$$

by asuming that the elemental abundance $Ab(X)$ is constant over the line of sight h. $C(T,\lambda_{ij},N_e)$, usually called the *contribution function*, is mostly a function of the electron temperature, and contains all the atomic parameters, and in particular the ionization fraction. N_H,N_e are the hydrogen and electron number densities. If we define the differential emission measure $DEM(T) = N_e N_H (dh/dT)$ we have:

$$I(\lambda_{ij}) = A_b(X) \int C(T,\lambda_{ij},N_e)\, DEM(T)\, dT \qquad (2)$$

from which in principle the relative element abundance $A_b(X_1)/A_b(X_2)$ of two elements X_1 and X_2 can be deduced from the observed intensity ratio I_1/I_2.
The best available atomic data, stored in the CHIANTI database (v.2, [9]) have been used here.

Most authors use various approximations to express the above equation in an even simpler way. These approximations were introduced about 30 years ago, when the uncertanties in the instrument's calibrations and in the atomic data were much larger than they are now. These approximations had the advantage of being computationally simple. In what follows, we briefly review these approximations, and outline the more correct approach that has been adopted here.

Following [10], many authors have approximated the expression for the line intensity by removing an averaged value of C(T) from the integral:

$$I = A_b(X)\ < C(T) > \int N_e N_H dh \qquad (3)$$

An emission measure $EM_L = I_{\rm ob}/(A_b(X) < C(T) >)$ can therefore be immediatly calculated for each observed line of intensity $I_{\rm ob}$. We define here the EM_L the line emission measure. The values $A_b(X)\ EM_L$ are plotted at the temperature $T_{\max}$ (defined as the temperature where $C(T)$ has a maximum), and the relative abundances derived in order to have all the points of the various ions lie along a common smooth curve. The differences between the various methods are related to the way the average $< C(T) >$ is calculated. Most authors follow the approximation given in [11].

A different approximation was proposed by [12]. The idea is to define for each observed line of intensity $I_{\rm ob}$ a single DEM value, that for clarity we define here as the *line* Differential Emission Measure DEM_L:

$$DEM_L \equiv \left\langle N_e N_H \frac{dh}{dT} \right\rangle \equiv \frac{I_{\rm ob}}{A_b(X)\ \int\ C(T) dT} \qquad (4)$$

A plot of the $A_b(X)\ DEM_L = I_{\rm ob}/\int\ C(T)dT$ values displayed at the temperatures $T_{\max}$ is used to derive the relative element abundances, by adjusting them in order to have a continuous sequence of values.

The more accurate approach adopted here is to use the largest possible number of lines, calculate the contribution functions at the measured densities, and then determine the relative element abundances and the DEM at the same time. In this way, most of the uncertainties will be reduced, and systematic effects highlighted.

Since the lines observed by CDS are produced by many ions covering a large temperature range, it is possible to deduce a DEM curve for each element, and to determine relative element abundances, by normalizing the DEM curves of the different elements. It should be mentioned that the determination of the DEM distribution is an ill-conditioned problem [see, e.g., 13, and references therein] where solutions are not unique, thus producing some added uncertainty. However, the conditioning can be improved with an appropiate line selection. All the low temperature lines (T $\leq 10^{5.5}$ K) observed by CDS/NIS are from high-FIP elements (N, O, Ne) while all the high temperature lines (T $\geq 10^{5.9}$ K) are from low-FIP elements (Mg, Ca, Fe, Si, Al). It is therefore possible to deduce the relative abundances within these two groups of lines. The scaling between the high and low-FIP elements can be done (see [14] for applications to quiet Sun and coronal hole observations) using lines that overlap in temperature. CDS/GIS observations are important, because GIS observes many other lines and ions that extend the overlapping region between the high- and low-FIP ions. This is particularly important, since the use of different ions from different isoelectronic sequences can help to indicate where the atomic physics is in disagreement with the observations (see, e.g., [4]).

An example

Here, the Skylab coronal hole cell-centre data of [15] are used as an example. The photospheric [16] abundances were used, together with the [17] ionization balance. The DEM distribution was derived using an inversion technique. The DEM method indicated the need to modify the O, Na, and Ca abundances by -0.2, +0.4, +0.2 (dex), respectively. Figure 1 shows the DEM_L values (left), and the DEM distribution (right). The DEM_L values are plotted at the temperature $T_{\max}$, while the points in the DEM curve are plotted at the effective temperature $\log\, T_{eff} = \int C(T)\ DEM(T)\ \log T\ dT / (\int C(T)\ DEM(T)\ dT)$, that is an average temperature more indicative of where the bulk of the emission is. In both cases the points have been calculated with photospheric abundances [16], to show the sensitivity of these

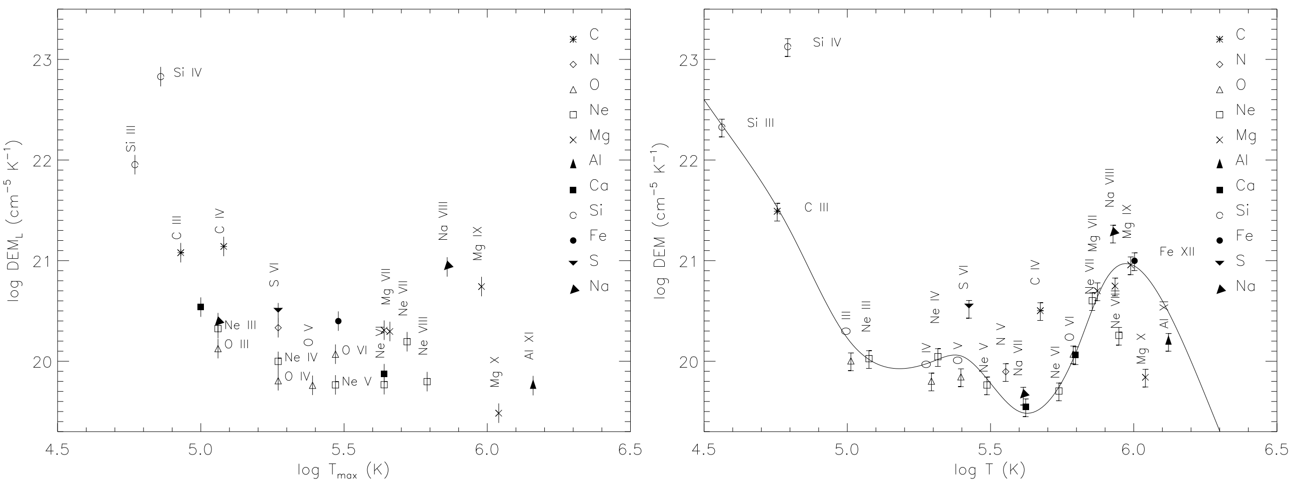

FIGURE 1. Left: line differential emission measures DEM_L of the selected lines plotted at the temperature T_{max}. Right: the *DEM* distribution, with each experimental data point plotted at the effective temperature T_{eff} and at a value equal to the product $DEM(T_{\mathrm{eff}})\mathrm{x}(I_{ob}/I_{th})$. The error bars represent an indicative 20% error on the observed intensities [15].

methods in measuring relative abundances.

For some lines, the DEM_L and *DEM* methods are in agreement. For example, they both clearly indicate the need to decrease the adopted O/Ne abundance (see e.g., the O IV and Ne IV points), and the fact that the Ne VIII and Mg X points are in total disagreement with the others. It is interesting to note that the photospheric abundance of O cited by [16] is 8.93 (log value), and if we assume fixed the Ne abundance, both methods indicate an oxygen abundance of 8.73, exactly the same value that has only recently been revised by [18].

However, in other cases the two methods produce very different results. For example, the DEM_L method does not indicate any need to modify the Na abundance, since the Na VIII point lies along a common smooth curve (neglecting Ne VIII, see below). On the other hand, the intensity of the Na VIII line, calculated with the *DEM*, is lower than the observed ones, by a factor of more than 2. How can the *DEM* and DEM_L methods differ by factors of more than 2 ? Only when the two lines have similar $C(T)$ and are emitted over a similar range of temperatures, can one assume the *DEM* to be constant and write:

$$\frac{\int C_1(T,N_e)\, DEM(T)\, dT}{\int C_2(T,N_e)\, DEM(T)\, dT} = \frac{\int C_1(T,N_e)\, dT}{\int C_2(T,N_e)\, dT} \qquad (5)$$

If the above equality holds, then it is possible to deduce the relative abundances directly from the observed intensities and the contribution functions, because:

$$\frac{A_b(X_1)}{A_b(X_2)} = \frac{I_1 \cdot \int C_2(T,N_e)\, dT}{I_2 \cdot \int C_2(T,N_e)\, dT} = \frac{DEM_L(X_2)}{DEM_L(X_1)} \qquad (6)$$

i.e., the *DEM* and DEM_L methods are equivalent. In any other case (defined here as the *DEM* effect), the two methods obviously produce different results. The *DEM* effect is particularly important when the emission $C(T)\ DEM(T)$ of a line peaks at temperatures where there is a non-negligible *DEM* gradient and Equation 5 does not hold. In the example produced here, the *DEM* distribution is such that the Na abundance estimate is mostly affected. However, other solar region observed have very different *DEM* distributions, and is impossible to know *a priori* if the approximation proposed by [12] is valid or not. These authors used their method to derive the Mg/Ne abundance of an erupting prominence, using Mg VI and Ne VI lines. A *DEM* analysis of this observation, performed by [5], has shown that the *DEM* peaks at $T = 10^{5.7}$ K, i.e. at the same temperature where the $C(T)$ of the Mg VI and Ne VI lines peaks. There is no *DEM* effect in this case, and the approximation used by [12] is therefore perfectly valid.

Another difference in the *DEM* and DEM_L methods is in the use of a different temperature at which the points are plotted. Note that there are substantial differences between T_{max} and T_{eff} for some lines. This can occur for example when the bulk of the emission comes from plasma at temperatures far from T_{max} (e.g. when there is a strong *DEM* gradient) or when the observed lines are blends of spectral lines that have $C(T)$ that peak at different temperatures.

TEMPERATURE (*DEM*) AND DENSITY EFFECTS

TABLE 1. Table of two Mg/Ne theoretical intensity ratios, calculated assuming A_b (Ne/Mg) = 0.5, for two densities N_e and: a) with a constant *DEM*; b) with a coronal hole plume *DEM* [19]; c) with a quiet Sun (network) *DEM* [14]. The values calculated in [20] (W F) for $N_e = 10^{10}$ and those presented by [21] (S) are also displayed for comparison in the last two columns. Note that the Mg VI 403.3 Å line is blended with a Ne VI line.

	$N_e = 10^8$	$N_e = 10^{10}$	$N_e = 10^{10}$ W F	S
Mg VI 400.666 Å /Ne VI 401.926 Å				
a) No *DEM*	1.50	0.90	0.97	1.00
b) Plume *DEM*	3.03	1.76	-	-
c) QS *DEM*	2.28	1.34	-	-
Ne VI 401.926 Å /Mg VI (+ Ne VI) 403.3 Å				
a) No *DEM*	0.40	0.65	-	0.61
b) Plume *DEM*	0.21	0.36	-	-
c) QS *DEM*	0.28	0.46	-	-

It is well known [3] that the Mg VI contribution functions are slightly skewed towards higher temperatures, when compared to the Ne VI ones. It is interesting to see the importance of the *DEM* effect here. Table 1 present two Mg VI / Ne VI theoretical intensity ratios, calculated assuming a constant *DEM* and using two *DEM* distributions, of a coronal hole plume and a quiet Sun. The Mg VI and Ne VI lines in Table 1 have been widely used by many authors [see, e.g., 21], because they are close in wavelength and because they have similar $C(T)$. The values in Table 1 show that if the *DEM* effect is neglected, the Ne/Mg relative abundance can be substantially underestimated, thus overestimating the FIP effect up to a factor of 3 (in the case of the plume). The *DEM* effect is much more pronounced when other line ratios such as Ca IX / Ne VII and Mg VII / Ne VII are considered, because their $C(T)$ peak at temperatures (log $T = 5.9$) where the *DEM* gradient is usually large. The small differences in their $C(T)$ are amplified when forming the integrals. Most of previous works on element abundances have neglected the shape of the *DEM* distribution when calculating the relative abundances, and it is therefore possible that some previous estimates were wrong by factors of 3 or more.

The Mg VI lines considered here are slightly density-dependent. Density variations can therefore change the observed Mg VI / Ne VI intensity ratios aswell. Table 1 also shows the effect that different densities have on the Mg/Ne intensity ratios. Transition region densities are difficult to measure, and usually different line ratios produce different values [see, e.g., 20]. The densities adopted for the calculation should be considered as extreme values, in the sense that measured transition region densities are $N_e = 1 \pm 0.5\text{x}10^9$ cm^{-3} [5]. Table 1 shows that the *DEM* effect is more important than the density effect. However, inaccurate estimates of densities can lead to non-negligible effects, up to 50%.

PROBLEMS WITH MANY IONS

The anomalous behaviour of the spectral lines of many ions, mostly of the Li and Na isoelectronic sequences was discussed in detail by [5] using Skylab data as well as SOHO/CDS and other data. If a *DEM* analysis is performed using lines from any other isoelectronic sequences, the theoretical intensities of the Li- and Na-like lines are under- or over-estimated by large factors, ranging from 2 up to 10. These discrepancies cannot be ascribed to element abundance anomalies, and actually give a strong warning against the use of these lines for *DEM* or element abundance analyses.

Anomalous behaviour of the Li-like and Na-like ions, was first reported by [22], using OSO-IV quiet Sun spectra. Such problems were not reported by [23] who used Skylab data. This can be explained by the fact that [23] mainly used Li-like lines (O VI, Ne VIII, Mg X, Si XII, S XIV) to constrain the *DEM* at high temperatures.

In the example presented here, the lines of the Li-like N V and C IV are underestimated by factors of 3 and 10, while those of Ne VIII and Mg X are overestimated by factors of 5 and 10, respectively. The S VI 933.3 Å (Na-like) is also underestimated by a factor of 3.

A *DEM* analysis of a rocket solar spectrum was presented by [24]. They found 'very significant and systematic differences' between the line intensities (by factors of 2 to 5) of the Li and Na isoelectronic sequences. A possible cause for this effect is a departure from ionization equilibrium, which can be explained with the long timescales of the dielectronic recombination from the He-like ions. Another possible cause could be due to inaccurate ionization equilibrium calculations.

A comparison between different ionization equilibrium calculations was reported by [5] for CDS observations of a simple quasi-isothermal region. Large differences were found, showing that the ionization balance plays a major role in the derivation of any element abundances, confirming the suggestions by [4]. In particular, [5] showed that if the more recent calculations of [25] are used instead of [17], the theoretical intensities of Ca IX and Ca X lines increase by factors of more than 3. If the ionization balance of [25] is used for the example shown here, significant differences for some of the ions are also found.

EXAMPLE OF CORONAL HOLE ABUNDANCES

Figure 2 shows ratios of selected lines of a CDS/GIS E-W scan across the Elephant's Trunk [14] coronal hole, when it was near disc centre, on 1996 August 27. The Mg VI / Ne VI and Ca IX / Ne VII ratios present variations that follow the cell-centre network pattern. The Mg VI/Ne VI values indicate, if no density and/or *DEM* effect are accounted for, an almost photospheric Ne/Mg abundance in the network regions (at Solar X=35, 70, 110 arcsec, where the ratio $\simeq 0.5$), with smaller values in the cell-centre regions (where the ratio $\simeq 0.9$).

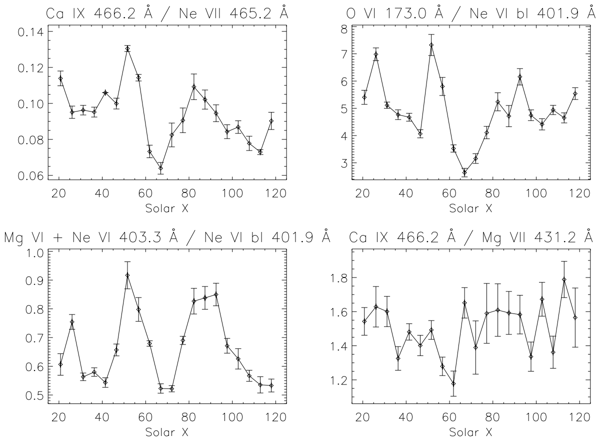

FIGURE 2. Intensity ratios (energy units) of selected lines of a CDS/GIS E-W scan across a coronal hole. The higher Mg VI / Ne VI values are located at the cell centres, at Solar X=50,90 arcsec

Can the higher Mg VI/Ne VI intensities in the cell-centres be explained instead by a density effect? Not really, since O IV measurements [5, 14] have indicated that the cell-centres have a higher electron density by about a factor of two. If this is true also for the heights where Mg VI is formed, then the Ne/Mg abundance would be slightly lower (and the FIP effect larger), since the Mg VI emissivity of the 403.3 Å line decreases with density. On the other hand, the higher Mg VI / Ne VI intensities can partly be explained by a temperature effect. Indeed, as shown in [14], the *DEM* distributions of the network and cell-centre regions are different, with the cell-centres having a steeper increase towards coronal temperatures.

However, an inspection of other combinations (Ca IX / Mg VII, O VI / Ne VI in Figure 2) suggests that most of these variations are probably due to a decreased Ne abundance in the cell centres which appears to occur relative to both low-FIP elements (Mg, Fe, Ca) and high-FIP ones (O). Variations of the Ne abundance, also relative to other high-FIP elements (such as O) have already been reported in a number of cases [19, 26].

CORONAL HOLE PLUMES

The most striking example in terms of a large Mg VI/Ne VI intensity ratio is given by coronal hole plumes. A large FIP bias (factor of 10) was derived by [27] from a Skylab off-limb EUV observation of a bright plume, using the DEM_L method and has long been thought that plumes have a large FIP effect. A *DEM* analysis was performed on the data tabulated in [27]. It showed that the plume had an isothermal distribution, similar to that one derived by [19] for an equatorial plume, and used as example in Table 1. The peak of the *DEM* was at $\log T = 5.9$, with a strong gradient where the $C(T)$ of the Ne VI and Mg VI lines differ most. The *DEM* effect here is so large that a photospheric Ne/Mg abundance can explain the Ne VI and Mg VI lines.

The fact that the large Mg VI/Ne VI intensity ratios observed in plumes are not indicative of a large FIP effect was also shown by [19], using SOHO/CDS observations. Here, we present further on-disc SOHO/CDS observations of a coronal hole plume to confirm this result. This plume was observed by CDS during the second week of October 1997 in the north polar hole. More details can be found in [5].

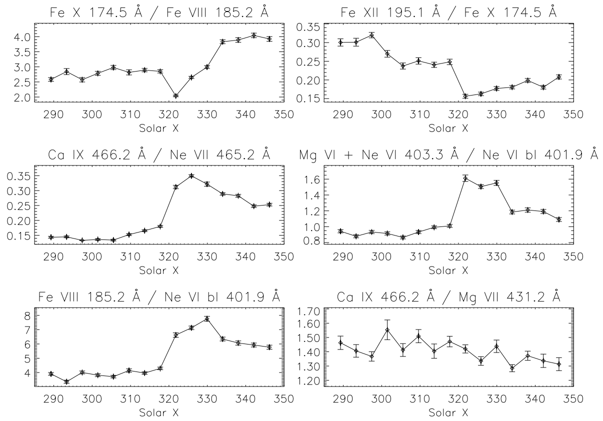

FIGURE 3. Intensity ratios (energy units) of few GIS lines during an E-W scan across a coronal hole plume (Solar X=320-330 arcsec).

A GIS scan was performed across the plume. Figure 3 shows how the intensity ratios of few GIS lines varies across the plume. The upper transition region lines have an increased intensity by a factor of about 4 in the plume area, while the high-temperature lines show a decreased intensity, indicating lower emission measures. There are indications of a density increase inside the plume area, as well as a decreased temperature. The Mg VI / Ne VI and Ca IX / Ne VII ratios show undoubtedly a large increase in the plume, and therefore a possibly large FIP effect. Nevertheless, an inspection of Fe VIII/Ne VI and

Ca IX / Mg VII ratios indicates that most of the observed variations are to be attributed to abundance variations of Ne only, as was observed for the equatorial plume [19]. Other ratios examined (e.g., Mg/Si) indicate that the relative abundances between the low-FIP elements remain almost unchanged.

If no density and *DEM* effects are considered, then the Mg/Ne abundance can be derived directly from the value of $\simeq 1.6$ of the Mg VI 403.3 Å / Ne VI 401.9 Å ratio (Figure 3). From Table 1 one derives (the inverse Ne VI/Mg VI value being 0.62) a Ne/Mg abundance of 0.5, and a large FIP effect of 6.8. The transition region density of that plume (as derived from Mg VII) was not much higher than the adjacent coronal hole network region, and therefore a density effect (that would increase the FIP effect) can be excluded.

A *DEM* analysis was performed on the plume area (Figure 3, $SolarX = 326''$), in order to determine its elemental abundance. The *DEM* peaks at $T = 7\text{x}10^5$ K with a quasi-isothermal distribution at these heights. The resulting FIP effect is less than 2, similar to the values found by [28, 29].

CONCLUSIONS

The derivation of element abundances from spectroscopic measurements is a complex issue. Many factors can affect the determination of the element abundances. Only some of those concerning observations of the low corona have been mentioned here, with few examples given. It is confirmed that coronal holes have photospheric abundances, while plumes only show a small FIP effect, contrary to what has long been thought. Clearly, some factors such as the ionization balance used, the selection of lines, and the *DEM* effect can each account for a variation of a factor of two or more in the derived element abundances, and should be given full consideration. Many problems, some of which are not of common knowledge in the astrophysical community, have been highlighted. If the problem with the Li-like ions is related to departures from ionization equilibrium, then it is likely that a large amount of work based on these ions in solar and stellar coronal physics will have to be revisited.

ACKNOWLEDGMENTS

Financial support from PPARC is acknowledged. We thank the CDS team for their support in the instrument operations. SOHO is a project of international cooperation between the European Space Agency and NASA.

REFERENCES

1. Raymond, J. C., et al., *this issue* (2001).
2. Mason, H. E., “Abundance determination in the quiet corona”, in *Proceedings of the First SOHO Workshop*, 1992, pp. 297–304.
3. Phillips, K. J. H., *Advances in Space Research*, **20**, 79 (1997).
4. Young, P. R., and Mason, H. E., *Space Science Reviews*, **85**, 315 (1998).
5. Del Zanna, G., Ph.D. thesis, Univ. of Central Lancashire, UK (1999).
6. Harrison, R. A. et al., *Sol. Phys.*, **162**, 233 (1995).
7. Young, P. R., and Mason, H. E., *Sol. Phys.*, **175**, 523–539 (1997).
8. Del Zanna, G., Bromage, B. J. I., Landi, E., and Landini, M., *A&A*, submitted (2001).
9. Landi, E., Landini, M., Dere, K. P., Young, P. R., and Mason, H. E., *Astron. Astrophys. Suppl. Ser.*, **135**, 339–346 (1999).
10. Pottasch, S. R., *Astrophys. J.*, **137**, 945 (1963).
11. Jordan, C., and Wilson, R., *ASSL Vol. 27: Physics of the Solar Corona*, p. 219 (1971).
12. Widing, K. G., and Feldman, U., *Astrophys. J.*, **344**, 1046–1050 (1989).
13. McIntosh, S. W., *Astrophys. J.*, **533**, 1043–1052 (2000).
14. Del Zanna, G., and Bromage, B. J. I., *J. Geophys. Res.*, **104**, 9753–9766 (1999).
15. Vernazza, J. E., and Reeves, E. M., *Astrophys. J. Suppl. Ser.*, **37**, 485–513 (1978).
16. Grevesse, N., and Anders, E., Solar interior and atmosphere. Tucson, AZ, University of Arizona Press, 1991, pp. 1227–1234.
17. Arnaud, M., and Rothenflug, R., *Astron. Astrophys. Suppl. Ser.*, **60**, 425–457 (1985).
18. Grevesse, N., *Adv. Space Res.*, in press (2001).
19. Del Zanna, G., and Bromage, B. J. I., *Space Science Reviews*, **87**, 169–172 (1999).
20. Widing, K. G., and Feldman, U., *Astrophys. J.*, **416**, 392 (1993).
21. Sheeley, N. R., *Astrophys. J.*, **469**, 423 (1996).
22. Dupree, A. K., *Astrophys. J.*, **178**, 527–542 (1972).
23. Raymond, J. C., and Doyle, J. G., *Astrophys. J.*, **247**, 686–691 (1981).
24. Judge, P. G., Woods, T. N., Brekke, P., and Rottman, G. J., *Astrophys. J. Letters*, **455**, L85 (1995).
25. Mazzotta, P., Mazzitelli, G., Colafrancesco, S., and Vittorio, N., *Astron. Astrophys. Suppl. Ser.*, **133**, 403–409 (1998).
26. Schmelz, J. T., Saba, J. L. R., Ghosh, D., and Strong, K. T., *Astrophys. J.*, **473**, 519 (1996).
27. Widing, K. G., and Feldman, U., *Astrophys. J.*, **392**, 715–721 (1992).
28. Young, P. R., Klimchuk, J. A., and Mason, H. E., *Astron. Astrophys.*, **350**, 286–301 (1999).
29. Wilhelm, K., and Bodmer, R., *Space Science Reviews*, **85**, 371–378 (1998).